Weak electronic correlations in the kagome superconductor AV_3Sb_5 (A = K, Rb, Cs)

Min Liu,[1,*] Zhiwei Wang,[1,2] and Jin-Jian Zhou[1,†]

[1]*Key Laboratory of Advanced Optoelectronic Quantum Architecture and Measurement (MOE), Beijing Key Lab of Nanophotonics, and Ultrafine Optoelectronic Systems, and School of Physics, Beijing Institute of Technology, Beijing 100081, People's Republic of China*

[2]*Material Science Center, Yangtze Delta Region Academy of Beijing Institute of Technology, Jiaxing 314011, People's Republic of China*

(Received 8 April 2022; revised 16 May 2022; accepted 2 June 2022; published 21 June 2022)

The kagome metals AV_3Sb_5 (A = K, Rb, Cs) have recently received enormous attention as they exhibit nontrivial topological electronic structure, flat band, unconventional intertwined charge density wave (CDW), anomalous Hall effect, and superconductivity. However, it is still controversial whether or not electronic correlations play an important role in these novel phenomena. Here we perform an extensive investigation on AV_3Sb_5 (A = K, Rb, Cs) with density functional theory plus dynamical mean field theory calculations. Our results indicate the electronic correlations effects are in the weak regime in both the normal state and the CDW state. The value of effective mass-enhancement m^*/m_{DFT} is about 1.3, and it is barely changed at temperatures ranging 50–900 K in the normal state. Our static susceptibility calculations with the normal structure show that static susceptibility has a weak q_z dependence and the Fermi-surface nesting mechanism does not work in this system. In the CDW state with the inverse Star of David structure, the spectral function opens a CDW gap at the Fermi level below T_{CDW} (50 K) compared with the normal state above T_{CDW} (300 K). We find that there exists orbital multiplicity at the Fermi level owing to two nonequivalent V atoms in CDW states, which may have an important role in forming the CDW order.

DOI: 10.1103/PhysRevB.105.235130

I. INTRODUCTION

The kagome lattice is formed by the tiled triangles and hexagons in a two-dimensional plane. It hosts a lot of novel physical phenomena, such as geometrical frustration, quantum spin liquid, charge density waves (CDW), flat band, Dirac cones, Weyl semimetals, and unconventional superconductivity [1–7]. Recently, the kagome superconductors AV_3Sb_5 (A = K, Rb, Cs) have received enormous attention as they show nontrivial topological electronic structure, anomalous Hall effect, unconventional intertwined charge density wave (CDW), and superconductivity [8–20]. However, the microscopic origin of the CDW and superconductivity is still under debate and controversial mechanisms are proposed.

Recent experiments observed CDW in AV_3Sb_5 (A = K, Rb, Cs) with the transition temperature at 80–110 K which is far above the superconducting transition temperature at 0.9–2.7 K [8–11]. Hard-x-ray scattering experiment by Li *et al.* found that the CDW in AV_3Sb_5 is an unconventional and electronic-driven mechanism, and they excluded the mechanism of strong electron-phonon coupling (EPC) driven CDW in AV_3Sb_5 [21]. However, recent angle-resolved photoemission spectroscopy (ARPES) [22], optical spectroscopy [23], and neutron scattering experiments [24] revealed that the CDW order in AV_3Sb_5 is associated with lattice distortion and not just a pure electronic instability, which means that EPC leads to the CDW. For the superconductivity, many experimental measurements, including the spin-lattice relaxation ($^{121/123}$Sb nuclear quadrupole resonance and ^{51}V NMR) [25], magnetic penetration depth [26], muon spin spectroscopy (μSR) [27], and ARPES measurements [22] show this system is conventional superconductor. But thermoelectric transport and scanning tunneling microscopy (STM) measurements indicate the system is unconventional superconductor [15–17,28–30]. Recent calculations on the normal state of KV_3Sb_5 suggests conventional superconductivity due to weak electronic local correlations in this system [31]. Despite these controversial conclusions, there is one consensus that the electronic correlations play an important role in unconventional CDW and superconductivity.

In this work, we performed a comprehensive study of the correlated electronic structure of AV_3Sb_5 in both the normal state and the CDW state using the density functional theory plus dynamical mean field (DMFT) method [32,33], taking KV_3Sb_5 as a study case. We find that the AV_3Sb_5 system exhibits weak electronic correlations in both the normal state and the CDW state, consistent with previous work [31]. The mass enhancement m^*/m_{DFT} ($1/Z$) in AV_3Sb_5 is about 1.3, which is much smaller than the typical value of 6–7 in strongly correlated materials, such as iron-based, cuprate superconductors, and heavy fermion materials. The temperature dependent electronic structure of AV_3Sb_5 has also been systematically studied. Above the CDW temperature, the electronic structure and mass enhancement of the normal state barely change

*minliu@bit.edu.cn
†jjzhou@bit.edu.cn

with temperature. Below the CDW temperature, we study the CDW state with an inverse Star of David (hexagon) structure; the electronic structure opens a CDW gap at the Fermi level comparing with the normal state. In order to understand the mechanism of the CDW, we did static susceptibility calculation, which shows static susceptibility has a weak q_z dependence and the Fermi-surface nesting mechanism does not work in this system. We find there exists orbital multiplicity at the Fermi level owing to two nonequivalent V atoms (V1 has the hexagon surrounding and V2 has triangle enclosing) in CDW states, which may have an important role in forming the CDW order. The weak electronic correlations in AV_3Sb_5 indicates they are conventional superconductors.

II. METHOD

We obtain DFT electronic structures of KV_3Sb_5 based on the full-potential augmented plane-wave method with the generalized gradient approximation (GGA) exchange-correlation functional by Perdew, Burke, and Ernzerhof (PBE) [34], as implemented in the WIEN2K code [35]. The muffin-tin radii are 2.50, 2.50, and 2.65 a.u. for K, V, and Sb, respectively. The maximum modulus for the reciprocal vector $K_{\max}$ was chosen such that $\mathrm{RMT}^* K_{\max} = 8.0$. All calculations were converged on a grid of 3000 k points in the irreducible Brillouin zone. A grid of 50 000 k points is adopted for the CDW calculation. And the structural relaxations were carried out using VASP [36,37]. For VASP calculations, the cutoff energy of 300 eV is chosen with the exchange-correlation functional of GGA-PBE. The projected augmented wave is adopted as the pseudopotentials [38]. We employ a $17 \times 17 \times 10$ k mesh for the CDW structure relaxation calculations. The DFT-D3 correction is employed to take in account the interlayer van der Waals interactions [39]. The lattice constants and internal coordinates are optimized until the atomic forces become less than 10^{-4} eV/Å.

We performed fully charge self-consistent DFT + DMFT calculations to treat the electronic correlations of V-3d orbitals using the EDMFT package [33], which is based on the full-potential linear augmented plane-wave method implemented in the WIEN2K code. The hybridization expansion continuous-time quantum Monte Carlo (CT-HYB) was used as the impurity solver [40]. V-3d local orbitals were constructed using projectors with an energy window from -10 to 10 eV relative to the Fermi energy. The Coulomb interaction was chosen to be $U = 5$ eV and $J_H = 0.7$ eV, we get the parameter from $SrVO_3$ and $CaVO_3$, which are correlated metals [41–43]. A nominal double-counting scheme with $n_f = 3.0$ was used. The self-energy in real frequency was obtained by analytic continuation based on the maximum entropy [44,45].

III. RESULT AND DISCUSSION

A. Crystal structure

The crystal structure for KV_3Sb_5 crystallizes in the hexagonal structure having a layered structure with the space group of $P6/mmm$. The V atoms form a kagome lattice with the kagome plane sandwiched by two layers of Sb1 atoms, and the Sb2 atoms which lie in the V-Sb plane [Fig. 1(a)]. The calculated lattice constants are $a = b = 5.41$ Å, $c = 8.89$ Å.

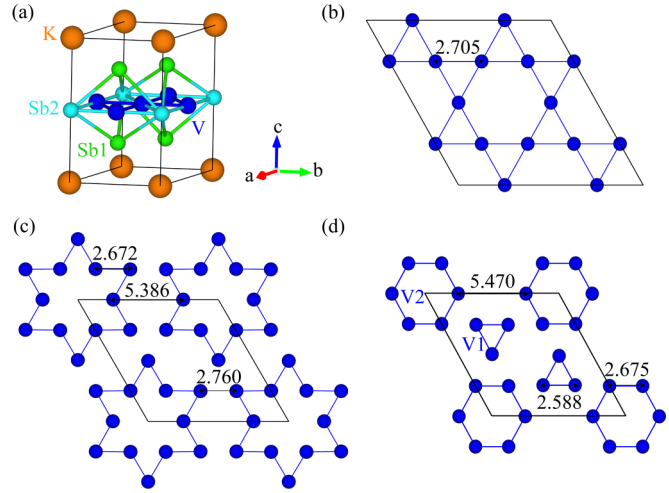

FIG. 1. (a) Crystal structure of KV_3Sb_5. The $2 \times 2 \times 1$ supercell of KV_3Sb_5 in normal state (b), Star of David structure (c), and inverse Star of David structure (d), respectively.

The atom positions are K (0.5, 0,0.5), V (0, 0, 0), Sb1 (1/3, 2/3, 0.7566), and Sb2 (0, 0, 0.5), respectively. In order to study the CDW state, we build a $2 \times 2 \times 1$ supercell [Fig. 1(b)] and slightly displace the V and Sb ions' position. After structural relaxation, the supercell converges to a structure of the Star of David [Fig. 1(c)] or the inverse Star of David (hexagon) [Fig. 1(d)]. And there exists two nonequivalent V atoms in the inverse Star of David structure as seen in Fig. 1(d). For the normal state, the kagome layer has an identical nearest neighbor V-V bond length $d_{\text{V-V}} = 2.705$ Å. But for the Star of David structure and the inverse Star of David structure, it shows different V-V bond lengths. We find that the inverse Star of David structure has a lower energy than the Star of David structure by 6 meV, which indicates that the CDW favors the former structure. This result is in good agreement with the experiments that the CDW structure is hexagon style structure [21–24].

B. Electronic structure of normal state

In order to quantify the electronic correlations effects of the V-d orbital, we calculate the effective mass enhancement m^*/m_{DFT}, which is equal to $1/Z$, and Z is the quasiparticle weight $Z = 1/(1-\frac{\partial \mathrm{Im}\Sigma(i\omega_n)}{\partial \omega_n}|_{\omega_n \to 0})$. The effective mass enhancement is a straightforward and quantitative way to characterize the strength of electronic correlations. The value of m^*/m_{DFT} is almost unity for weakly correlated systems, but often greater than 1 in strongly correlated systems. For example, the typical value of effective mass enhancement in cuprate superconductors and d electron heavy fermion materials is about 6–7 [46–48]. Figure 2(a) shows the computed mass enhancement m^*/m_{DFT} in KV_3Sb_5 with different values of Coulomb interaction U ranging 2–10 eV with Hund interaction J fixed at 0.7 eV, and Fig. 2(b) shows the m^*/m_{DFT} by varying the Hund interaction J from 0.0 to 0.9 eV with U fixed at 5.0 eV. For a typical U of 5.0 eV and J of 0.7 eV that are commonly used for $SrVO_3$ and $CaVO_3$ [41–43], our computed value of m^*/m_{DFT} in KV_3Sb_5 is 1.320, 1.258, 1.440, 1.280, and 1.287 for V-d_{z^2}, V-$d_{x^2y^2}$, V-d_{xz}, V-d_{yz}, and

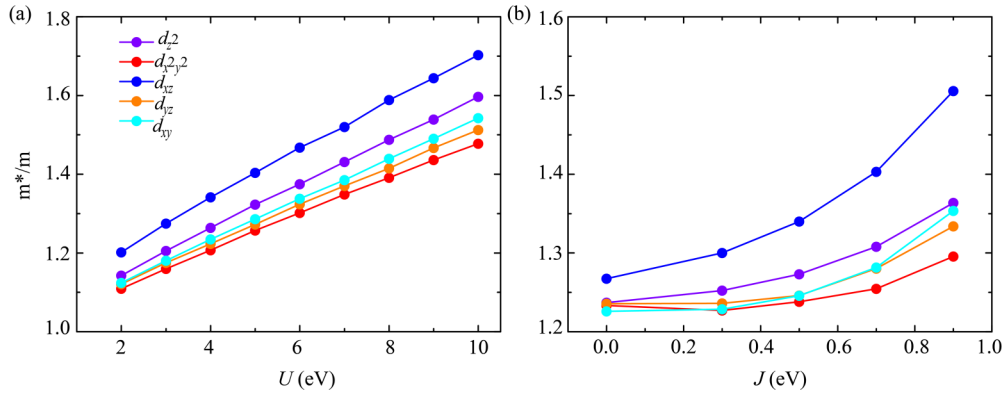

FIG. 2. The mass enhancement m^*/m_{DFT} of KV_3Sb_5 with different values of Coulomb interaction U and Hund interaction J in (a) and (b), respectively. The value of J is fixed at 0.7 eV in (a), while the value of U is fixed at 5.0 eV in (b).

V-d_{xy} at 300 K, respectively (see Table I). We also study the electronic correlations effects in RbV_3Sb_5 and CsV_3Sb_5: the m^*/m_{DFT} is almost average at 1.30 of the V-d orbitals which are similar with KV_3Sb_5. These results are in good agreement with resent ARPES measurements [49] and indicate that the electronic correlations are weak in this system.

Figure 3 shows our computed electronic structure of KV_3Sb_5. The metallic ground state is in good agreement with experimental data [8,9]. The computed DFT band structure and DFT + DMFT quasiparticle dispersion are very close to each other near the Fermi level. One can observe from the projected band structure, as shown in Fig. S1 of the Supplemental Material [50], that the bands near the Fermi level are mainly contributed by the V-d and Sb-p orbitals. There are four Van Hove singularities (VHSs) near the Fermi level in the vicinity of the M point with B_{2g} and A_g symmetry. These VHSs are mainly contributed by V-d_{xy}, V-d_{xz}, V-d_{z^2}, and V-$d_{x^2y^2}$ orbitals. The electron pocket located at the Gamma point is mainly Sb_2-p_z orbital character. At K and H points, the band structure shows two Dirac points about 0.5 eV below the Fermi level. A kagome lattice induced flat band with V-d_{yz} orbital character occurs at 1.0 eV below the Fermi level, which is expected from the tight-binding model calculation [51]. However, in our DMFT calculation at $T = 300$ K [Fig. 3(a)], the flat band is pushed down to 0.75 eV. Besides, our DMFT result presents an additional flat band of V-d_{xy} character at about -1.25 eV along Γ-M-K, which indicates strong band renormalization due to the electronic correlations effects of the V-d orbital. This result is consistent with the experimental observation

TABLE I. DFT + DMFT calculations of the effective mass enhancement m^*/m_{DFT} of KV_3Sb_5 evolve with different temperatures.

	m^*/m_{DFT}				
Temperature	d_{z^2}	$d_{x^2y^2}$	d_{xz}	d_{yz}	d_{xy}
50	1.3503	1.3312	1.4154	1.2936	1.5164
100	1.3198	1.3079	1.4089	1.2890	1.5042
200	1.3152	1.2529	1.4018	1.2725	1.3054
300	1.3192	1.2536	1.3913	1.2614	1.2903
600	1.3244	1.2557	1.4033	1.2740	1.2937
900	1.3237	1.2571	1.4043	1.2742	1.3024

[49]. A similar trend can be found in the DMFT spectral functions of RbV_3Sb_5 and CsV_3Sb_5 as shown in Fig. S2 [50].

The effects of spin-orbital coupling (SOC) are usually very important in the kagome lattice. Figure 3(b) shows the electronic structure of KV_3Sb_5 computed with SOC. Comparing to Fig. 3(a), the significant change induced by SOC is the gap opening of the Dirac cone located at K and H points about 0.3 eV below the Fermi level. The electronic structure near the Fermi level is barely affected. Therefore, the SOC effect is neglected in the following discussion.

The imaginary part of hybridization functions in KV_3Sb_5 have been studied in both Matasubara and real frequency as shown in Figs. S3 and S4 [50]. Five orbitals of imaginary hybridization in Matasubara frequency appear delocalized at low frequency. We can get the same result in real frequency, and it shows that V-d_{z^2} and V-d_{xy} have a strong hybridization with Sb-p orbital at the low frequency. We have also investigated the imaginary part of the Matsubara self-energy and the real part of the real frequency self-energy in KV_3Sb_5, as shown in Figs. S3(b) and S4(b) [50], respectively. The imaginary self-energy does not have a quasiparticle peak near ω equal to zero, which means the quasiparticle lifetime is short. Our results demonstrate that KV_3Sb_5 is a weakly correlated metal. From our DFT + DMFT calculations, the orbital resolved V-3d occupation n_d is 3.218. The occupation of d_{z^2}, $d_{x^2y^2}$, d_{xz}, d_{yz}, and d_{xy} is 0.709, 0.456, 0.572, 0.548, and 0.933, respectively. To further validate the weak correlated effect, we also compare the PDOS with DFT and DMFT results as shown in Figs. S5 and S6 [50], which shows little reconstruction near the Fermi level; only the d electrons are moving to the Fermi level.

As in strong correlated metals, temperature effects usually have a major role in the band reconstruction. So, we also study the temperature effect on the electronic structure. The spectral functions are almost the same as the temperature varies from 50, 100, 200, 300, 600, and 900 K in the normal state. Here, we show the imaginary part of self-energy of the V-d orbital in Matsubara frequency which evolves with the temperature. It is found that the imaginary part of Matsubara self-energy in the V-d_{z^2} orbital is almost unchanged from 50 to 300 K, similar to other V-d orbitals as shown in Fig. 4, which means KV_3Sb_5 has weak electronic correlations effect in the normal state. From Table I, it shows that the effective mass

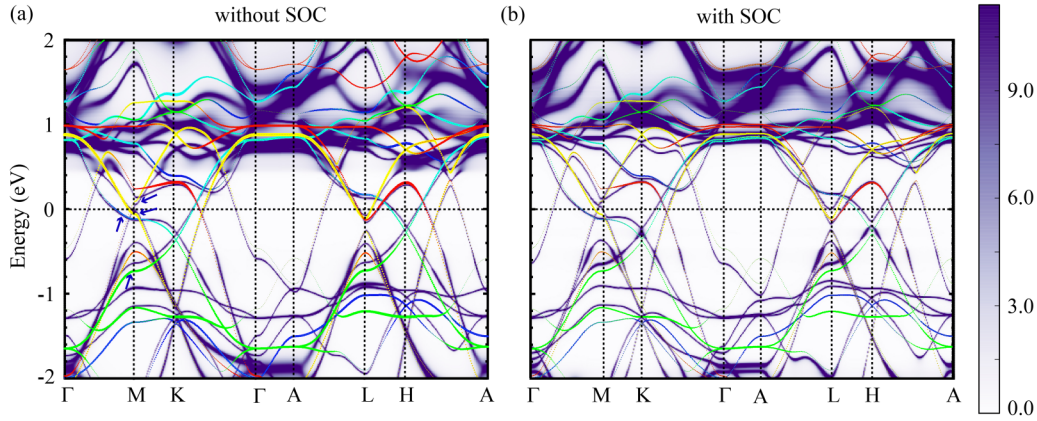

FIG. 3. DFT + DMFT spectral functions of KV_3Sb_5 at 300 K computed (a) without and (b) with SOC. For comparison, the corresponding DFT band structures are plotted in color lines (the blue color is V-d_{z^2}, cyan is V-$d_{x^2y^2}$, yellow is V-d_{xz}, red is V-d_{yz}, and green is V-d_{xy}). The zero of the energy axis is the Fermi level. Four VHSs near the Fermi level in the vicinity of M point are indicated with blue arrows.

enhancement m^*/m_{DFT} of KV_3Sb_5 evolves with different temperatures using the DFT + DMFT method. But the value of m^*/m_{DFT} presents little changes, which further indicates that the kagome lattice KV_3Sb_5 has weak electronic correlations. The weak electronic correlations in AV_3Sb_5 indicates that they are conventional superconductors.

C. Charge density wave

Recent experiments show evidence of an intertwined charge density wave (CDW) phase in KV_3Sb_5. However, the underlying mechanism is still controversial. The CDW mechanisms can be generally divided into three categories [52]: The first one is the weak coupling scenario based on Fermi-surface instabilities, in which segments of Fermi contours are connected by q_{CDW} Fermi-surface nesting (FSN). The FSN results in the effective screening of phonons and induces Kohn anomalies in phonon dispersion at q_{CDW}, driving a lattice restructuring at low temperature. The second one is the strong coupling scenario, in which the CDW is derived from strong electron-electron interactions or electron-phonon interactions. A typical example is 2H-$NbSe_2$ [53], where the momentum

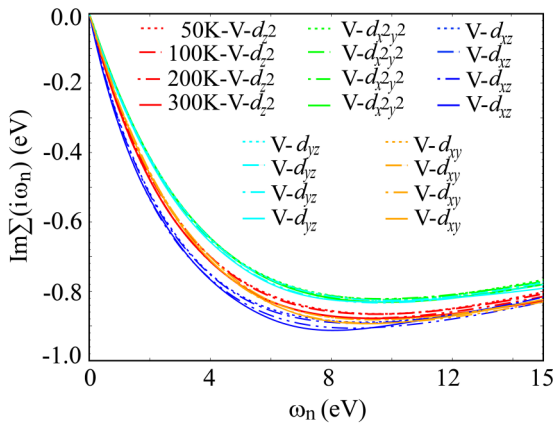

FIG. 4. The imaginary part of Matsubara self-energy in KV_3Sb_5 at different temperatures of $T = 50, 100, 200, 300$ K computed using the DFT + DMFT method.

dependence of the electron-phonon coupling (EPC) matrix element determines the characteristic of the CDW phase. And in cuprates and iron-based unconventional superconductors, the CDW phase belongs to the third category; it means that neither FSN nor EPC directly lead to the CDW. In addition, neither phonon softening nor lattice instability near T_{CDW} is observed. The mechanism is still unclear, though it is speculated that the antiferromagnetic and the Coulomb correlation interactions may play a key role [52]. As for the AV_3Sb_5, it draws different opinions with different experiments. On one hand, it was said that the FSN and VHSs have led to the CDW [21]. On the other hand, the EPC leads to the CDW [22]. However, neither of them considered the electronic correlations effect in CDW.

Hence, in our work we study the CDW including electronic correlations effects. First, we calculate the Fermi surface using the DFT and DFT + DMFT methods. We obtained the quasiparticle band structure via a low-energy quasiparticle Hamiltonian, described as $H_{\mathrm{QP}} = H_0 - \mu + \mathrm{Re}\Sigma(\omega = 0)$, where H_0 is the noninteraction Hamiltonian from DFT and $\mathrm{Re}\Sigma(\omega = 0)$ is the real part of the real frequency self-energy at $\omega = 0$. We diagonalize H_{QP} to obtain the quasiparticle band structure, which is then used to determine the Fermi surface. This approach has been widely employed and validated in previous works [54]. We have checked that the quasiparticle band structure obtained from the above approach is consistent with the quasiparticle peak of the spectral functions near the Fermi level. The computed Fermi surfaces are shown in Fig. 5. One can observe that there are two bands crossing the Fermi level both in DFT [Figs. 5(a) and 5(b)] and DFT + DMFT [Figs. 5(c) and 5(d)]. The first band shows almost the same result between the two methods as seen in Figs. 5(a) and 5(c), which indicates the weak electronic correlations effects in this material. The cylinder electron pocket in the center is the Sb2-p_z orbital. The other bands are almost the V-d orbital. And from the first band, it shows that the $3Q$ [$Q1$(0.5, 0), $Q2$(0.5, 0.5), $Q3$(0. 0.5)] Fermi-surface nesting vector connects the three M points, where we can also find three VHSs. However, the second band's Fermi surface shape shows little difference along the k_z (Γ-A) direction, which means DMFT has little band construction correction. It contributes little to the whole

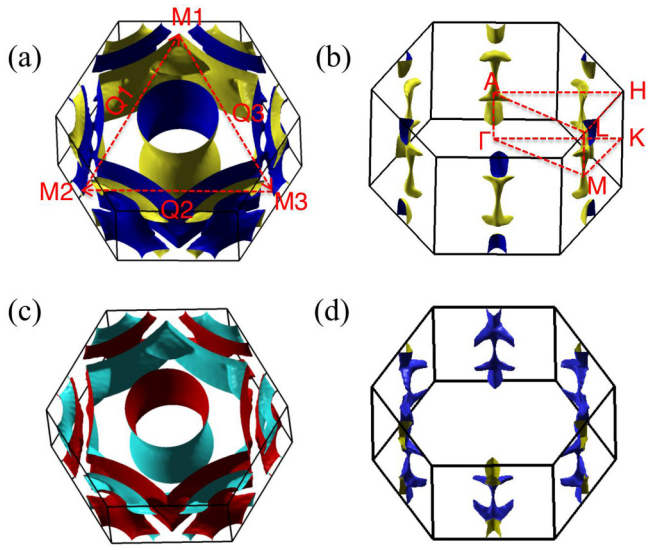

FIG. 5. Fermi surface of KV_3Sb_5. Panels (a) and (b) are the DFT result, (c) and (d) are DFT + DMFT results.

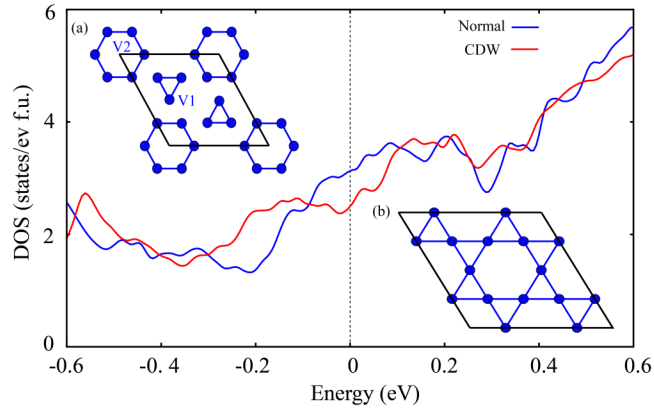

FIG. 7. The DFT + DMFT density of states of normal state at $T = 300$ K and CDW state at $T = 50$ K; the inner structures (a) and (b) are the CDW and normal state structures, respectively.

Fermi surface. Hence, from the Fermi surface results also present the weak electronic correlations in KV_3Sb_5.

In order to further investigate the CDW state, we also consider the Lindhard static susceptibility χ_0 to study the Fermi surface nesting. The real part of the χ_0 reveals the quantity for a CDW instability. $\chi_0(q,\omega) = \sum_{\iota\iota',k} \frac{f(\epsilon_{\iota k})-f(\epsilon_{\iota' k+q})}{\varepsilon_{\iota k}-\varepsilon_{\iota' k+q}-\omega-i\eta}$, here $f(\varepsilon)$ is the Fermi function and $\varepsilon_{\iota k}$ is the quasiparticle eigenenergies. The Fermi temperature and k points were well tested to convergence. Here the Fermi-temperature smearing of T equals 9 meV and we use a fine k mesh of $46 \times 46 \times 25$–$50\,000$ k points in the Brillouin zone. The smearing of $\eta = 1.0 \times 10^{-4}$. As shown in Fig. 6, at $q_z = 0$, it was found that the maxima of the χ_0 is located between the Γ and K points ($1/2\Gamma K$), which indicates there exists CDW instability at $1/2\Gamma K$ when q_z equals zero. However, $1/2\Gamma K$ is not a Fermi-surface nesting vector, which means we can rule out the Fermi-nesting mechanism in CDW order. And from $q_z = 0.25$ to $q_z = 0.5$, it also shows that the maximum of the χ_0 changes slightly, and the static susceptibility has a weak dependent q_z.

D. Electronic structure of CDW state

We also investigate the electronic structure of the CDW state, which has an inverse Star of David structure below T_{CDW} as shown in Fig. 1(d). Here, we also did the calculations with the $2 \times 2 \times 2$ supercell of an inverse Star of David structure, but it changes little compared with the $2 \times 2 \times 1$ supercell. Hence, we just show the result of the $2 \times 2 \times 1$ supercell. Based on this structure, the orbital occupation has changed, the total V-3d occupation n_d is 3.202, for d_{z^2}, $d_{x^2y^2}$, d_{xz}, d_{yz}, and d_{xy} is 0.5362, 0.6397, 0.5594, 0.9228, and 0.5436, respectively. The V-3d_{xy} occupation has changed a little compared with the normal state. Based on this structure, we calculate the partial density of states (PDOS) of the normal state structure and the CDW state structure using the DFT + DMFT method (Fig. 7). It shows a CDW gap near the Fermi level, which is also in agreement with the experiment and previous DFT calculations [23]. The CDW states show two different sites of V atoms. V1 has the hexagon surrounding and V2 has the triangle enclosing. The PDOS of the CDW states in DFT and DFT + DMFT both show that V1 and V2 have different orbital character as shown in Fig. 8. V1 has d_{xz} and $d_{x^2y^2}$ orbital at the Fermi level, but V2 has d_{xy} and d_{z^2} orbital character. The orbital multiplicity at the Fermi level, namely multiple orbitals' contribution to the electronic structure at the Fermi level, might be one of the reasons leading to the CDW order. The orbital multiplicity effects in the

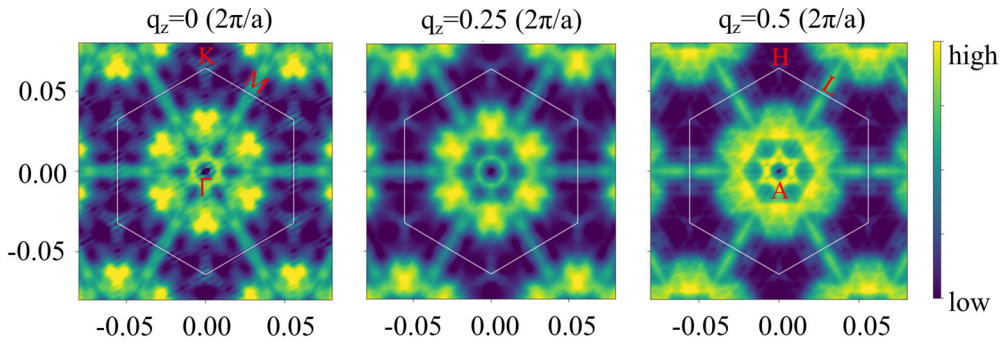

FIG. 6. DFT + DMFT calculation of the real Lindhard susceptibility χ_0 in KV_3Sb_5 along with the q_z direction.

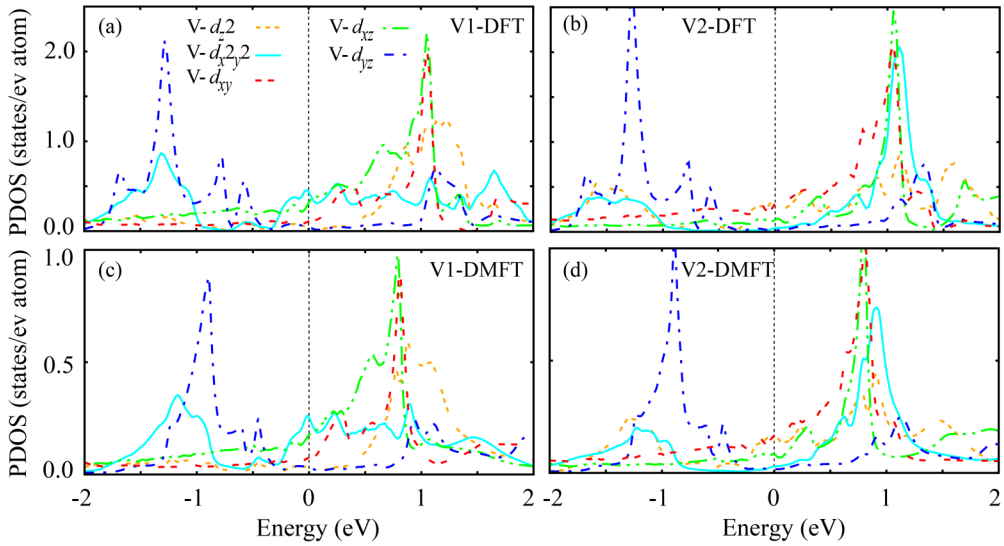

FIG. 8. The DFT and DFT + DMFT calculations of partial density of states (PDOS) for the CDW state.

formation of CDW have been discussed previously in cuprate superconductors and $NbSe_2$, in which a single-band model fails to depict their CDW behaviors. Flicker and Wezel [55,56] proposed a two-band model to study the CDW order and find that the multiband effects are crucial in the formation of CDW order [57]. The in-depth analysis of the connections between orbital multiplicity and formation of CDW in KV_3Sb_5 will be the subject of future work.

IV. CONCLUSION

We investigated the electronic structure of the kagome metals AV_3Sb_5 (A = K, Rb, Cs) using density functional theory plus dynamical mean field theory. Our results show that AV_3Sb_5 have weak correlated electronic interactions, which can be manifested from the quasiparticle renormalization factor Z or the mass enhancement m^*/m_{DFT} ($1/Z$). The m^*/m_{DFT} is around at 1.3, which is much smaller than the typical value of strongly correlated materials. The evolution of electronic structure with temperatures have also been investigated. The imaginary part of the self-energy of the V-d orbital in Matsubara frequency barely changes in the normal state as the temperature increase from 50 to 900 K, which again demonstrates that this system has weak electronic correlated effects. The Fermi surface changes slightly at temperature above the CDW temperature in the normal state. We studied the CDW state below the T_{CDW} (∼50 K) with the inverse Star of David structure by the $2 \times 2 \times 1$ supercell using the DFT + DMFT method, where we found a CDW gap in the electronic spectral function. In order to explain the mechanism of the CDW, we performed static susceptibility calculations and found that static susceptibility has a weak q_z dependence and the Fermi-surface nesting mechanism does not work in this system. But there exists orbital multiplicity at the Fermi level owing to two nonequivalent V atoms in CDW states, which may have an important role in forming the CDW order. The weak electronic correlations in AV_3Sb_5 demonstrated in our work suggests that they are conventional superconductors.

ACKNOWLEDGMENTS

The authors thank Y. Xu and Y. Wang for the fruitful discussion. This work was supported by the National Natural Science Foundation of China (Grants No. 92065109 and No. 12104039) and the Beijing Municipal Natural Science Foundation (Grant No. Z210006).

[1] A. P. Ramirez, Strongly geometrically frustrated magnets, Annu. Rev. Mater. Sci. **24**, 453 (1994).

[2] S. Yan, D. A. Huse, and S. R. White, Spin-Liquid ground state of the s = 1/2 kagome heisenberg antiferromagnet, Science **332**, 1173 (2011).

[3] W.-S. Wang, Z.-Z. Li, Y.-Y. Xiang, and Q.-H. Wang, Competing electronic orders on kagome lattices at van hove filling, Phys. Rev. B **87**, 115135 (2013).

[4] N. J. Ghimire and I. I. Mazin, Topology and correlations on the kagome lattice, Nat. Mater. **19**, 137 (2020).

[5] L. Ye, M. Kang, J. Liu, F. v. Cube, C. R. Wicker, T. Suzuki, C. Jozwiak, A. Bostwick, E. Rotenberg, D. C. Bell *et al.*, Massive dirac fermions in a ferromagnetic kagome metal, Nature (London) **555**, 638 (2018).

[6] N. Morali, R. Batabyal, P. Kumar Nag, E. K. Liu, Q. N. Xu, Y. Sun, B. H. Yan, C. Felser, N. Avraham, and H. Beidenkopf, Fermi-arc diversity on surface terminations of the magnetic weyl semimetal Co_3Sn_2S, Science **365**, 1286 (2019).

[7] M. L. Kiesel, C. Platt, and R. Thomale, Unconventional Fermi Surface Instabilities in the Kagome Hubbard Model, Phys. Rev. Lett. **110**, 126405 (2013).

[8] B. R. Ortiz, L. C. Gomes, J. R. Morey, M. Winiarski, M. Bordelon, J. S. Mangum, I. W. H. Oswald, J. A. R. Rivera, J. R. Neilson, S. D. Wilson *et al.*, New kagome prototype materials: Discovery of KV_3Sb_5, RbV_3Sb_5, and CsV_3Sb_5, Phys. Rev. Materials **3**, 094407 (2019).

[9] B. R. Ortiz, P. M. Sarte, E. M. Kenney, M. J. Graf, S. M. L. Teicher, R. Seshadri, and S. D. Wilson, Superconductivity in

the Z_2 kagome metal KV_3Sb_5, Phys. Rev. Materials **5**, 034801 (2021).

[10] Q. Yin, Z. Tu, C. Gong, Y. Fu, S. Yan, and H. Lei, Superconductivity and normal-state properties of kagome metal RbV_3Sb_5 single crystals, Chin. Phys. Lett. **38**, 037403 (2021).

[11] B. R. Ortiz, S. M. L. Teicher, Y. Hu, J. L. Zuo, P. M. Sarte, E. C. Schueller, A. M. M. Abeykoon, M. J. Krogstad, S. Rosenkranz, R. Osborn *et al.*, CsV_3Sb_5: A Z_2 Topological Kagome Metal with a Superconducting Ground State, Phys. Rev. Lett. **125**, 247002 (2020).

[12] S.-Y. Yang, Y. J. Wang, B. R. Ortiz, D. F. Liu, J. Gayles, E. Derunova, R. G. Hernandez, L. Smejkal, Y. L. Chen, S. S. P. Parkin *et al.*, Giant, unconventional anomalous Hall effect in the metallic frustrated magnet candidate, KV_3Sb_5, Sci. Adv. **6**, eabb6003 (2020).

[13] Y.-X. Jiang, J.-X. Yin, M. M. Denner, N. Shumiya, B. R. Ortiz, J. He, X. Liu, S. S. Zhang, G. Chang, I. Belopolski *et al.*, Unconventional chiral charge order in kagome superconductor KV_3Sb_5, Nat. Mater. **20**, 1353 (2021).

[14] F. H. Yu, D. H. Ma, W. Z. Zhuo, S. Q. Liu, X. K. Wen, B. Lei, J. J. Ying, and X. H. Chen, Unusual competition of superconductivity and charge-density-wave state in a compressed topological kagome metal, Nat. Commun. **12**, 3645 (2021).

[15] N. Shumiya, M. S. Hossain, J.-X. Yin, Y.-X. Jiang, B. R. Ortiz, H. Liu, Y. Shi, Q. Yin, H. Lei, S. S. Zhang *et al.*, Intrinsic nature of chiral charge order in the kagome superconductor RbV_3Sb_5, Phys. Rev. B **104**, 035131 (2021).

[16] Z. Wang, Y.-X. Jiang, J.-X. Yin, Y. Li, G.-Y. Wang, H. L. Huang, S. Shao, J. Liu, P. Zhu, N. Shumiya *et al.*, Electronic nature of chiral charge order in the kagome superconductor CsV_3Sb_5, Phys. Rev. B **104**, 075148 (2021).

[17] H. Chen, H. T. Yang, B. Hu, Z. Zhao, J. Yuan, Y. Q. Xing, G. J. Qian, Z. H. Huang, G. Li, Y. H. Ye *et al.*, Roton pair density wave in a strong-coupling kagome superconductor, Nature (London) **599**, 222 (2021).

[18] H. Zhao, H. Li, B. R. Ortiz, S. M. L. Teicher, T. Park, M. X. Ye, Z. Q. Wang, L. Balents, S. D. Wilson, and I. Zeljkovic, Cascade of correlated electron states in the kagome superconductor CsV_3Sb_5, Nature (London) **599**, 216 (2021).

[19] K. Y. Chen, N. N. Wang, Q. W. Yin, Y. H. Gu, K. Jiang, Z. J. Tu, C. S. Gong, Y. Uwatoko, J. P. Sun, H. C. Lei *et al.*, Double Superconducting Dome and Triple Enhancement of Tc in the Kagome Superconductor CsV_3Sb_5 Under High Pressure, Phys. Rev. Lett. **126**, 247001 (2021).

[20] F. Du, S. S. Luo, B. R. Ortiz, Y. Chen, W. Y. Duan, D. T. Zhang, X. Lu, S. D. Wilson, Y. Song, and H. Q. Yuan, Pressure-induced double superconducting domes and charge instability in the kagome metal KV_3Sb_5, Phys. Rev. B **103**, L220504 (2021).

[21] H. X. Li, T. T. Zhang, Y.-Y. Pai, C. Marvinney, A. Said, T. Yilmaz, Q. Yin, C. Gong, Z. Tu, E. Vescovo *et al.*, Observation of Unconventional Charge Density Wave without Acoustic Phonon Anomaly in Kagome Superconductors AV_3Sb_5 (A = Rb,Cs), Phys. Rev. X **11**, 031050 (2021).

[22] H. L. Luo, Q. Gao, H. X. Liu, Y. H. Gu, D. S. Wu, C. J. Yi, J. J. Jia, S. L. Wu, X. Y. Luo, Y. Xu *et al.*, Electronic nature of charge density wave and electron-phonon coupling in kagome superconductor KV_3Sb_5, Nat. Commun. **13**, 273 (2022).

[23] E. Uykur, B. R. Ortiz, S. D. Wilson, M. Dressel, and A. A. Tsirlin, Optical detection of charge-density-wave instability in the non-magnetic kagome metal KV_3Sb_5, npj Quantum Mater. **7**, 16 (2022).

[24] Y. F. Xie, Y. K. Li, P. Bourges, A. Ivanov, Z. J. Ye, J.-X. Yin, M. Z. Hasan, A. Y. Luo, Y. G. Yao, Z. W. Wang *et al.*, Electron-phonon coupling in the charge density wave state of CsV_3Sb_5, Phys. Rev. B **105**, L140501 (2022).

[25] C. Mu, Q. W. Yin, Z. J. Tu, C. S. Gong, H. C. Lei, Z. Li, and J. L. Luo, S-Wave superconductivity in kagome metal CsV_3Sb_5 revealed by 121/123Sb NQR and 51V NMR measurements, Chin. Phys. Lett. **38**, 077402(2021).

[26] W. Y. Duan, Z. Y. Nie, S. S. Luo, F. H. Yu, B. R. Ortiz, L. C. Yin, H. Su, F. Du, A. Wang, Y. Chen *et al.*, Nodeless superconductivity in the kagome metal CsV_3Sb_5, Sci. China Phys. Mech. Astron. **64**, 107462 (2021).

[27] R. Gupta, D. Das, C. H. Mielke III, Z. Guguchia, T. Shiroka, C. Baines, M. Bartkowiak, H. Luetkens, R. Khasanov, Q. W. Yin *et al.*, Microscopic evidence for anisotropic multigap superconductivity in the CsV_3Sb_5 kagome superconductor, npj Quantum Mater. **7**, 49 (2022).

[28] C. C. Zhao, L. S. Wang, W. Xia, Q. W. Yin, J. M. Ni, Y. Y. Huang, C. P. Tu, Z. C. Tao, Z. J. Tu, C. S. Gong *et al.*, Nodal superconductivity and superconducting domes in the topological Kagome metal CsV_3Sb_5, arXiv:2102.08356.

[29] Z. W. Liang, X. Y. Hou, W. R. Ma, F. Zhang, P. Wu, Z. Y. Zhang, F. H. Yu, J.-J. Ying, K. Jiang, L. Shan *et al.*, Three-Dimensional Charge Density Wave and Robust Zero-Bias Conductance Peak Inside the Superconducting Vortex Core of a Kagome Superconductor CsV_3Sb_5, Phys. Rev. X **11**, 031026 (2021).

[30] H.-S. Xu, Y. J. Yan, R. T. Yin, W. Xia, S. J. Fang, Z. Y. Chen, Y. J. Li, W. Q. Yang, Y. F. Guo, and D.-L. Feng, Multiband Superconductivity with Sign-Preserving Order Parameter in Kagome Superconductor CsV_3Sb_5, Phys. Rev. Lett. **127**, 187004 (2021).

[31] J. Z. Zhao, W. K. Wu, Y. L. Wang, and S. Y. A. Yang, Electronic correlations in the normal state of kagome superconductor KV_3Sb_5, Phys. Rev. B **103**, L241117 (2021).

[32] A. Georges, W. Krauth, and M. J. Rozenberg, Dynamical mean-field theory of strongly correlated fermion systems and the limit of infinite dimensions, Rev. Mod. Phys. **68**, 13 (1996).

[33] G. Kotliar, S. Y. Savrasov, K. Haule, V. S. Oudovenko, O. Parcollet, and C. A. Marianetti, Electronic structure calculations with dynamical mean-field theory, Rev. Mod. Phys. **78**, 865 (2006).

[34] J. P. Perdew, K. Burke, and M. Ernzerhof, Generalized Gradient Approximation Made Simple, Phys. Rev. Lett. **77**, 3865 (1996).

[35] P. Blaha, K. Schwarz, G. K. H. Madsen, D. Kvasnicka, J. Luitz, R. Laskowski, F. Tran, and L. D. Marks, *WIEN2k, An Augmented Plane Wave + Local Orbitals Program for Calculating Crystal Properties* (Karlheinz Schwarz, Techn. Universität Wien, Vienna, Austria, 2019).

[36] G. Kresse and J. Furthmuller, Efficiency of ab-initio total energy calculations for metals and semiconductors using a plane-wave basis set, Comput. Mater. Sci. **6**, 15 (1996).

[37] G. Kresse and J. Furthmuller, Efficient iterative schemes for ab initio total-energy calculations using a plane-wave basis set, Phys. Rev. B **54**, 11169 (1996).

[38] P. E. Blochl, Projector augmented-wave method, Phys. Rev. B **50**, 17953 (1994).

[39] S. Grimme, J. Antony, S. Ehrlich, and H. Krieg, a consistent and accurate ab initio parametrization of density functional

dispersion correction (dft-d) for the 94 elements h-pu, J. Chem. Phys. **132**, 154104 (2010).

[40] E. Gull, A. J. Millis, A. I. Lichtenstein, A. N. Rubtsov, M. Troyer, and P. Werner, Continuous-time Monte Carlo methods for quantum impurity models, Rev. Mod. Phys. **83**, 349 (2011).

[41] E. Pavarini, S. Biermann, A. Poteryaev, A. I. Lichtenstein, A. Georges, and O. K. Andersen, Mott Transition and Suppression of Orbital Fluctuations in Orthorhombic 3d1 Perovskites, Phys. Rev. Lett. **92**, 176403 (2004).

[42] C. Taranto, M. Kaltak, N. Parragh, G. Sangiovanni, G. Kresse, A. Toschi, and K. Held, Comparing quasiparticle GW+DMFT and LDA+DMFT for the test bed material $SrVO_3$, Phys. Rev. B **88**, 165119 (2013).

[43] I. A. Nekrasov, G. Keller, D. E. Kondakov, A. V. Kozhevnikov, Th. Pruschke, K. Held, D. Vollhardt, and V. I. Anisimov, Comparative study of correlation effects in $CaVO_3$ and $SrVO_3$, Phys. Rev. B **72**, 155106 (2005).

[44] K. Haule, C.-H. Yee, and K. Kim, Dynamical mean-field theory within the full-potential methods: Electronic structure of $CeIrIn_5$, $CeCoIn_5$, and $CeRhIn_5$, Phys. Rev. B **81**, 195107 (2010).

[45] M. Jarrell and J. E. Gubernatis, Bayesian inference and the analytic continuation of imaginary-time quantum monte carlo data, Phys. Rep. **269**, 133 (1996).

[46] Z. P. Yin, K. Haule, and G. Kotliar, Kinetic frustration and the nature of the magnetic and paramagnetic states in iron pnictides and iron chalcogenides, Nat. Mater. **10**, 932 (2011).

[47] C. Weber, K. Haule, and G. Kotliar, Optical weights and waterfalls in doped charge-transfer insulators: A local density approximation and dynamical mean-field theory study of $La_{2-x}Sr_xCuO_4$, Phys. Rev. B **78**, 134519 (2008).

[48] M. Liu, Y. J. Xu, D. Q. Hu, Z. M. Fu, N. H. Tong, X. R. Chen, J. G. Cheng, W. H. Xie, and Y.-F. Yang, Symmetry-enforced heavy-fermion physics in the quadruple-perovskite $CaCu_3Ir_4O$, arXiv:1705.00846.

[49] Y. Hu, S. M. L. Teicher, B. R. Ortiz, Y. Luo, S. T. Peng, L. W. Huai, J. Z. Ma, N. C. Plumb, S. D. Wilson, J. F. He *et al.*, Charge-order-assisted topological surface states and flat bands in the kagome superconductor CsV_3Sb_5, Sci. Bull. **67**, 495 (2022).

[50] See Supplemental Material at http://link.aps.org/supplemental/10.1103/PhysRevB.105.235130 for the details of the projected band structure of KV_3Sb_5 in DFT and DFT + SOC calculations, DFT + DMFT spectral functions of AV_3Sb_5, imaginary part of Matsubara hybridization function and self-energy, imaginary part of real frequency hybridization function, real part of real frequency self-energy, DOS and PDOS of KV_3Sb_5 calculated with DFT and DMFT at 300 K.

[51] X. X. Wu, T. Schwemmer, T. Müller, A. Consiglio, G. Sangiovanni, D. D. Sante, Y. Iqbal, W. Hanke, A. P. Schnyder, M. M. Denner *et al.*, Nature of Unconventional Pairing in the Kagome Superconductors AV_3Sb_5, Phys. Rev. Lett. **127**, 177001 (2021).

[52] X. T. Zhu, Y. W. Cao, J. D. Zhang, E. W. Plummer, and J. D. Guo, Classification of the charge density waves based on their nature, Proc. Natl Acad. Sci. USA **112**, 2367 (2015).

[53] M. Calandra, I. I. Mazin, and F. Mauri, Effect of dimensionality on the charge-density wave in few-layer 2H-$NbSe_2$, Phys. Rev. B **80**, 241108(R) (2009).

[54] Y. S. Xu, J. J. Zhao, C. J. Yi, Q. Wang, Q. W. Yin, Y. L. Wang, X. L. Hu, L. Y. Wang, E. K. Liu, G. Xu *et al.*, Electronic correlations and flattened band in magnetic weyl semimetal candidate Co_3Sn_2S, Nat. Commun. **11**, 3985 (2020).

[55] F. Flicker and J. V. Wezel, Charge order form orbital-dependent coupling evidenced by $NbSe_2$, Nat. Commun. **6**, 7034 (2015).

[56] F. Flicker and J. van Wezel, Charge order in $NbSe_2$, Phys. Rev. B **94**, 235135 (2016).

[57] Á. Pásztor, A. Scarfato, M. Spera, F. Flicker, C. Barreteau, E. Giannini, J. van Wezel, and C. Renner, Multiband charge density wave exposed in a transition metal dichalcogenide, Nat. Commun. **12**, 6037 (2021).